Journal of
Materials Chemistry A

Accepted Manuscript

This article can be cited before page numbers have been issued, to do this please use: P. Zhou, D. Dang, M. Xiao, Q. Wang, J. Zhong, H. Tan, Y. Pei, R. Yang and W. Zhu, *J. Mater. Chem. A*, 2015, DOI: 10.1039/C5TA00166H.

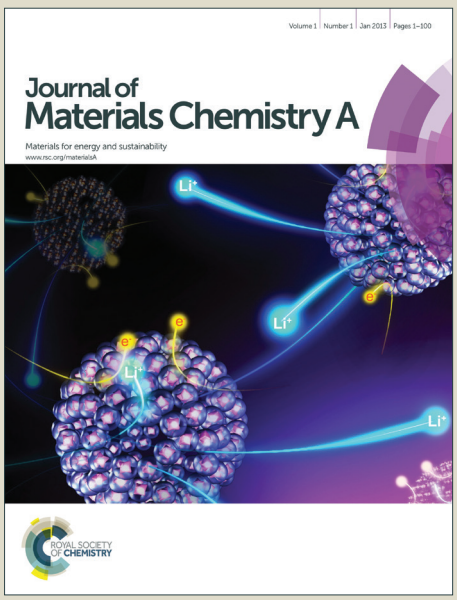

ROYAL SOCIETY OF CHEMISTRY

www.rsc.org/materialsA

View Article Online
DOI: 10.1039/C5TA00166H

Improved photovoltaic performance of star-shaped molecules with triphenylamine core by tuning substituted position of carbazolyl at terminal

Pei Zhou,[a] Dongfeng Dang,[a] Manjun Xiao,[a,b] Qiong Wang,[a] Juan Zhong,[a] Hua Tan,[a] Yong Pei,[a] RenqiangYang,[b*] Weiguo Zhu[a*]

[a] Department of Chemistry, Key Lab of Environment-Friendly Chemistry and Application in the Ministry of Education, Xiangtan University, Xiangtan 411105, P. R. China

[b]Qingdao Institute of Bioenergy and Bioprocess Technology, Chinese Academy of Sciences, Qingdao 266101, P. R. China

Corresponding author: Prof. Weiguo Zhu; Renqiang Yang

Tel: +86-731-58293377

Fax: +86-731-58292251

E-mail addresses: zhuwg18@126.com

View Article Online
DOI: 10.1039/C5TA00166H

Abstract:

Two star-shaped molecules of TPA(BT-2Cz)$_3$ and TPA(BT-3Cz)$_3$ with a triphenylamine (TPA) core were designed and synthesized, in which 2- and 3-carbazolyl units (2Cz and 3Cz) are attached to the benzothiadiazole (BT) arms as planar terminal groups, respectively. Although both molecules show a similar broad UV-Vis absorption covering from 300 nm to 560 nm, different photovoltaic performances were observed owing to the varied linked positions of terminal carbazolyl units. In contrast to TPA(BT-2Cz)$_3$-based solar cells, solution-processable organic solar cells (OSCs) based on TPA(BT-3Cz)$_3$ exhibited better photovoltaic performance with the maximum power conversion efficiency up to 3.94% and an enhanced short-circuit current of 8.80 mA cm^{-2}. This work further demonstrates that tuning the substituted position of terminal carbazolyl group can significantly improve the photovoltaic performance for its resulting small molecules.

Keywords:Organic solar cells, Star-shaped molecules, Photovoltaic performance, Carbazolyl, Triphenylamine.

View Article Online
DOI: 10.1039/C5TA00166H

1. Introduction

Solution processable organic solar cells (OSCs) exhibit great potential in large area applications for their advantages of low cost, light weight and capability in fabricating flexible devices.[1-4] Among them, bulk hetero-junction (BHJ) OSCs using small molecules (SMs) as donor materials are under intense investigation because these SMs have well-defined molecular structures, no end group contaminants, and good batch-to-batch reproducibility.[3-5] Currently, significant progress has been made for these SMs based organic solar cells (SM-OSCs) with the achievement of power conversion efficiency (PCE) up to 6%-10%.[6-10] However, in contrast to their polymer counterparts, SM-OSCs still show an inferior photovoltaic performance and some key parameters, such as short-circuit current density (J_{sc}) and fill factor (*FF*), have not been improved well.[11] Therefore, developing novel SMs with broad and strong absorption to sunlight, matched energy levels and high carrier mobility is still needed.[1-4] One facile strategy is to construct the D-A-type SMs using the proper electron-rich moiety (D) and electron-deficient moiety (A) forming the intra-molecular charge transfer (ICT).[12,13] On the other hand, the star-shaped molecules usually exhibited much stronger absorption and higher holes mobility than their linear counterparts, which could lead to an enhanced J_{sc} and PCE.[14] For instance, Li *et al* reported a series of the triphenylamine (TPA)-based SMs with different spatial configurations and found these SMs with three-armed configuration (t-TPA-BT) displayed not only a much broader and stronger absorption, but also a better photovoltaic performance than those bi-armed and linear molecules.[15] Based on the above consideration, the star-shaped D-A-type conjugated SMs are paid more and more attention currently.[16]

As known, TPA and its derivatives exhibited high holes mobility and good solution processability benefiting from their three-dimensional (3-D) spatial structure, and is widely used as a donor unit to construct the D-A type molecules for the applications in OSCs.[17-21] 2,1,3-Benzothiadiazole(BT) unit has been demonstrated to be a promising type of acceptor building block due to its good electron-withdrawing

View Article Online
DOI: 10.1039/C5TA00166H

nature.[22-25] Some researchers developed a type of star-shaped molecules containing both TPA and BT building blocks[22-24] and found that the increased photovoltaic performances were obtained by tuning terminal groups for these TPA-BT-based molecules. However, satisfactory result has not been made yet.

Recently, our group reported another star-shaped molecule containing the TPA central unit and diketopyrrolopyrrole (DPP) arms, and found that introducing planar terminal groups of phenanthrenes (PN) can enhance photovoltaic performances for this TPA-DPP-based molecule in OSCs significantly.[18] Based on this achievement, we try to design novel star-shaped TPA-BT-based molecules by introducing new planar terminal group in order to further improve their photovoltaic performance. As carbazolyl (Cz) unit has a planar molecular structure, good chemical and environmental stability,[26-28] furthermore, the topology, absorption, energy level and holes mobility of its SMs was found to be tuned easily by altering the carbazolyl coupling position in SMs.[29-31] Therefore, in this paper, we utilized TPA as core, BT as three arms and different substituted carbazolyl as terminal groups to design two star-shape molecules of TPA(BT-2Cz)$_3$ and TPA(BT-3Cz)$_3$, which bear 2-carbazolyl (2Cz) and 3-carbazolyl (3Cz) terminal groups, respectively. Similar thermal stability and UV-Vis absorption profile from 300 nm to 560 nm were observed for both SMs. However, compared to their counterparts, TPA(BT-2Cz)$_3$ showed lower HOMO energy level and TPA(BT-3Cz)$_3$ displayed higher charge carrier mobility. Significant effect of the substituted positions of carbazolyl on photovoltaic performance of its SMs was further observed in the device with a structure of ITO/PEDOT: PSS/Active Layer/Ca/Al. Better and improved photovoltaic performance was exhibited in the TPA(BT-3Cz)$_3$-based devices, in which the maximum PCE and J_{sc} values were 3.94% and 8.80 mA/cm^2, respectively. Our results further demonstrated that introducing terminal carbazolyl groups and tuning their linked positions could significantly improve the photovoltaic performance for its SMs in OSCs.

2. Experimental section

2.1.Materials

View Article Online
DOI: 10.1039/C5TA00166H

All reagents and chemicals were purchased from commercial sources (Aldrich, Acros, TCI) and used without further purification unless stated otherwise. Tetrahydrofuran (THF) was distilled over sodium and benzophenone under an inert nitrogen atmosphere. The detailed syntheses of 2-(7-bromobenzo[*c*][2,1,3]thiadiazol- 4-yl) -9-octylcarbazole(Br-BT-2Cz), 3-(7-bromobenzo[*c*][2,1,3]thiadiazol-4-yl)-9-octylcarbazole (Br-BT-3Cz) and tris(4-(4,4,5,5-tetramethyl-1,3,2-dioxaborolan-2-yl)phenyl) amine (TPA-3B) were outlined in Supporting Information.

2.2. Synthesis

2.2.1 Synthesis of TPA(BT-3Cz)$_3$

To a solution ofcompounds Br-BT-3Cz(280 mg, 0.56 mmol) and TPA-3B(70 mg, 0.11 mmol) in toluene (50 mL), anhydrous ethanol (10 mL) and potassium carbonate aqueous solution (2 M, 2 mL) was added tetrakis(triphenylphosphine)palladium [Pd-(PPh_3)$_4$] (25 mg) under nitrogen atmosphere. The mixture was stirred at 80 ^oC for 24 h. The reaction was then quenched with water at ambient temperature and the mixture was extracted with dichloromethane (DCM). The combined organic layer was dried over anhydrous magnesium sulfate ($MgSO_4$)and distilled to remove off the solvent. The residue was purified by column chromatography on silica gel using DCM and petroleum ether (PE) (*V/V*= 1:1) as the eluent to give an orange solid (78 mg, yield 48.15%). ^1H NMR (400 MHz, $CDCl_3$), δ (ppm): 8.72 (s, 3H), 8.22 (d, J = 15.5 Hz, 3H), 8.15 (d, J = 8.4 Hz, 3H), 8.04 (d, J = 7.6 Hz, 6H), 7.92 (d, 3H), 7.88 (d, J = 7.1 Hz, 3H), 7.59 (d, J = 7.3 Hz, 3H), 7.56–7.39 (m, 15H), 4.38 (t, J = 5.7 Hz, 6H), 2.24–1.69 (m, 6H), 1.49–1.13 (m, 30H), 0.98–0.80 (br, 9H). MALDI-MS (MSD, m/z) for $[M]^+$ $C_{96}H_{90}N_{10}S_3$, 1478.65; found, 1478.85.^{13}C NMR (100 MHz, $CDCl_3$), δ (ppm): 154.67, 154.23, 147.32, 140.97, 140.49, 133.94, 132.40, 131.68, 130.25, 128.33, 127.89, 127.85, 127.17, 125.92, 124.50, 123.29, 123.12, 121.33, 120.67, 119.11, 108.95, 108.80, 77.43, 77.11, 76.79, 43.30, 31.89, 29.78, 29.48, 29.27, 29.11, 27.41, 22.69, 14.17. Elemental analysis for $C_{96}H_{90}N_{10}S_3$: Calcd C, 77.94; H, 6.10; N, 9.47. Found C, 77.86; H, 6.21; N, 9.28.

2.2.2 Synthesis of TPA(BT-2Cz)$_3$

View Article Online
DOI: 10.1039/C5TA00166H

Compound TPA(BT-2Cz)$_3$ was synthesized according to the synthetic procedure of TPA(BT-3Cz)$_3$ as an orange solid with a yield of 50.60%.^{1}H NMR (400 MHz, $CDCl_3$), δ (ppm): 8.26 (d, J = 7.9 Hz, 1H), 8.17 (d, J = 7.5 Hz, 1H), 8.11 (s, 1H), 8.04 (d, J = 7.5 Hz, 2H), 7.95 (d, J = 6.9 Hz, 1H), 7.88 (d, J = 6.9 Hz, 1H), 7.82 (d, J = 8.0 Hz, 1H), 7.48 (dd, J = 15.8, 7.7 Hz, 4H), 7.28 (d, J = 10.3 Hz, 1H), 4.53–4.27 (br, 6H), 2.06–1.80 (br, 6H), 1.49–1.02 (m, 30H), 0.92–0.76 (br, 9H).MALDI-MS (m/z): 1478.85. MALDI-MS (MSD, m/z) for $[M]^+$ $C_{96}H_{90}N_{10}S_3$, 1478.65; found, 1478.73.^{13}C NMR (100 MHz, $CDCl_3$), δ (ppm): 154.58, 154.24, 147.41, 141.24, 140.73, 134.86, 133.95, 132.35, 132.33, 130.31, 128.48, 127.69, 125.95, 124.53, 122.99, 122.69, 120.63, 120.44, 120.18, 119.00, 109.95, 108.84, 77.40, 77.08, 76.76, 43.23, 31.87, 29.45, 29.25, 29.10, 27.42, 22.66, 14.12. Elemental analysis for $C_{96}H_{90}N_{10}S_3$: Calcd C, 77.94; H, 6.10; N, 9.47. Found C, 77.69; H, 6.28; N, 9.34.

2.3. Characterization and measurement

All ^{1}H NMR and ^{13}C NMR spectra were recorded on a Bruker AV-400 using $CDCl_3$ as solvent. MALDI-TOF mass spectrometric measurements were performed on BrukerBifiex III MALDI TOF. The theoretical study was performed using the density functional theory (DFT), as approximated by the B3LYP employing the 6-31G** basis set in Gaussian09. UV-Vis spectra were measured on a Perkin-Elmer Lamada 25 spectrometer. Thermogravimetric analyses (TGA) were performed on a Netzsch TG 209 analyzer and differential scanning calorimeter (DSC) was measured on a TA Q200 Instrument under nitrogen atmosphere at a heating rate of 20 ^{o}C min^{-1}. Cyclic voltammograms (CV) were performed with a three-electrode electrochemical cell in a 0.1 M tetra(n-butyl)ammonium hexafluorophosphate ($TBAPF_6$) solutionwith a scan 100 mV s^{-1} at room temperature under argon atmosphere. A platinum wire and Ag/AgCl (0.1 M) were used as counter electrode and reference electrode, respectively. The thin films on the Pt disk, formed by drop-casting the molecular chloroform solution (analytical reagent, 10 mg/mL) in the disk, was used as the working electrode. Surface morphologies were recorded by atomic force microscopy (AFM) on a Veeco-DI Multimode NS-3D apparatus in a trapping mode under normal air condition at room temperature.

View Article Online
DOI: 10.1039/C5TA00166H

2.4. Fabrication and characterization of organic solar cells

The photovoltaic cells were made with a traditional sandwich structure through the following steps. Firstly, the indium tin oxide (ITO)-coated glass substrates were cleaned by a series of ultrasonic treatments in acetone, following by deionized water, then 2-propanol each for 10 min. The substrates were dried under a stream of nitrogen and subjected to the treatment of Ar/O_2 plasma for 5 min. Secondly, a filtered aqueous solution of poly(3,4-ethylenedioxy-thiophene)-poly(styrenesulfonate) (PEDOT:PSS; Bayer AG) was spun-cast onto the cleaned ITO surface at 4000 rpm for 30 s and then baked at 150 ^{o}C for 30 min to form a PEDOT: PSS thin film with a thickness of 30 nm. Thirdly, a blend solution of materials and [6,6]-phenyl-C-71-butyric acid methyl ester ($PC_{71}BM$) in chlorobenzene (CB), filtered through a 0.45 μm poly(tetrafluoro-ethylene) filter, was spun cast at 2000 rpm for 30 s onto the PEDOT: PSS layer. The substrates were dried under N_2 atmosphere at room temperature and then annealed at 150 ^{o}C for 15 min in a nitrogen-filled glove box. The devices were completed after thermal deposition of a 10 nm calcium and a 100 nm aluminum film as the cathode at a pressure of 6×10^{-4} Pa. The active area was 0.1 cm^2 for each cell. The thicknesses of the spun-cast films were recorded by a profilometer (Alpha-Step 200; Tencor Instruments).

Current density-voltage (*J-V*) characteristics of devices were measured by a computer-controlled Keithley 2602 source measurement unit in the dark under an AM 1.5 G irradiation at an intensity of 100 mW cm^{-2} (Oriel 91160, 300 W). PCE was detected under a monochromatic illumination (Oriel Cornerstone 260 1/4 m monochromator equipped with Oriel 70613NS QTH lamp) and the calibration of the incident light was performed with a single-crystalline silicon diode. External quantum efficiency (*EQE*) was measured with a silicon photodiode and a computer-controlled light source-monochromator-lock-in system. All device measurements were carried out in air at room temperature.

3. Results and discussion

3.1. Synthesis and thermal stability

View Article Online
DOI: 10.1039/C5TA00166H

The synthetic routes of TPA(BT-2Cz)$_3$ and TPA(BT-3Cz)$_3$are outlined in Scheme 1. As the key precursors of both star-type molecular arms, 2-(7-bromobenzo[*c*][2,1,3] thiadiazol-4-yl)-9-octyl carbazole (Br-BT-2Cz) and 3-(7-bromobenzo[*c*][2,1,3]thia-diazol-4-yl)-9-octylcarbazole (Br-BT-3Cz) were prepared through the common Suzuki coupling reaction using Pd(PPh$_3$)$_4$ as the catalyst (See Supporting Information). Similarly, TPA(BT-2Cz)$_3$ and TPA(BT-3Cz)$_3$ were easily obtained through Suzuki coupling reaction in a moderate yield of 50%. Two target SMs were confirmed well with ^{1}H NMR, ^{13}C NMR, TOF-MS and elemental analysis. Like the other star-type molecules, both TPA(BT-2Cz)$_3$ and TPA(BT-3Cz)$_3$ are readily dissolved in the common organic solvents, such as DCM, chloroform ($CHCl_3$) and chlorobenzene (CB) at the room temperature.

The thermal properties of both molecules were evaluated with thermogravimetric analysis (TGA) and differential scanning calorimeter (DSC). The recorded TGA and DSC curves are depicted in Fig S1 (a) and (b), respectively (See Supporting Information). Their corresponding data are summarized in Table 1. The thermal decomposition temperatures of 469 ^{o}C and 463 ^{o}C are observed for TPA(BT-2Cz)$_3$ and TPA -(BT-3Cz)$_3$ with a 5% weight loss, respectively, implying that both molecules have good thermal properties. On the other hand, no distinct endothermic and exothermic peaks are exhibited for TPA(BT-3Cz)$_3$ during the heating and cooling processes. However, an endothermic peak at 246 °C and exothermic peak at approximately 208 °C are observed for TPA(BT-2Cz)$_3$, indicating that different crystalline properties were obtained by altering the linking position of the terminal carbazolyl.

3.2 Theoretical calculations

The ground-state geometry of TPA(BT-2Cz)$_3$ and TPA(BT-3Cz)$_3$ was fully optimized by density functional theory (DFT) at the B3LYP/6-31G** level and an ethyl group was used instead of octyl group to make the calculation easier. The minimum-energy conformations and electron-state-density distributions are represented in Fig. 1. The dihedral angles between phenyl of TPA and BT, as well as between BT and Cz for TPA(BT-3Cz)$_3$ are calculated to be 34.71^o and 34.83^o, respectively, which are much

View Article Online
DOI: 10.1039/C5TA00166H

smaller than those corresponding dihedral angles in TPA(BT-2Cz)$_3$, indicating that TPA(BT-3Cz)$_3$ has more planar molecular structure than TPA(BT-2Cz)$_3$. Therefore, TPA(BT-3Cz)$_3$ is expected to have better π-π stacking than TPA(BT-2Cz)$_3$ and exhibit the increased J_{sc} and PCE values.[32] In addition, the electron density of HOMO of TPA(BT-3Cz)$_3$ is delocalized on the whole molecule and such a delocalization is much less for TPA(BT-2Cz)$_3$. As a result, TPA(BT-3Cz)$_3$ could have a slightly increasing HOMO energy level in comparison with TPA(BT-2Cz)$_3$. On the other hand, the electron density of LUMO for both molecules is mainly localized on the BT units, which is consistent with the reported literatures.[25,33]

3.3 Optical properties and electrochemical properties

The UV-Vis absorption spectra of TPA(BT-2Cz)$_3$ and TPA(BT-3Cz)$_3$ in chloro-form solution and solid films are shown in Fig. 2 and their corresponding absorption data are listed in Table 1. By employing carbazole as the terminal, broad absorption spectra from 300 nm to 570 nm with two obvious absorption peaksare observed. The high-lying region at about 320 nm corresponds to the π-π* transition and the low-lying region from 400 to 550 nm is assigned to the intra-molecular charge transfer (ICT) interaction between electron-rich moiety (Cz and TPA) and electron-deficient moiety (BT).[32,34] Compared to the absorption profiles in solution, those ones in thin films exhibited significant red-shift up to 24~30 nm, which is probably caused by intermolecular π-π stacking interaction. The similar absorption spectra for both SMs in solutions and thin films imply that the substituted position of carbazole has little effect on the absorption spectra.

Fig. 3 shows the cyclic voltammetry (CV) curves of TPA(BT-2Cz)$_3$ and TPA(BT-3Cz)$_3$ and their correlate data are also listed in Table 1. The potentials are internally calibrated using the ferrocene/ferrocenium of the (Fc/Fc^+) redox couple (4.8 eV below the vacuum level). The HOMO and LUMO energy levels (E_{HOMO} and E_{LUMO}) are calculated to be -5.25 eV/ -3.24 eV for TPA(BT-2Cz)$_3$ and -5.18 eV/ -3.15 eV for TPA(BT-3Cz)$_3$ from the onset oxidation potential (E_{ox}) and the onset reduction

View Article Online
DOI: 10.1039/C5TA00166H

potential (E_{red}) according to the referenced equations.[35] It is noticed that TPA(BT-2Cz)$_3$ have a deeper HOMO energy level, which is consistent with our DFT calculation result using the B3LYP/6-31G** model. The lower E_{HOMO} value should be available for TPA(BT-2Cz)$_3$ to exhibit higher V_{oc} in OSCs.

3.4 Photovoltaic performance

To probe the photovoltaic properties of both star-shaped molecules, single bulk heterojunction organic solar cells were fabricated by solution process with a structure of ITO/PEDOT: PSS/Active Layer/Ca/Al under an optimal spin-coating rate of 2000 rpm. As demonstrated, the blend ratios (*w*/*w*) in photoactive layer could affect the photovoltaic performance of OSCs seriously,[36] therefore, the blend ratios between SMs to $PC_{71}BM$ were optimized primarily here, as shown in Fig. S2. The optimized blend ratio of 1:4 was obtained for both molecules-based solar cells. Fig. 4 displays the current density-voltage (*J*-*V*) characteristics of TPA(BT-2Cz)$_3$ and TPA(BT-3Cz)$_3$-based OSCs in the optimized conditions under illumination of AM 1.5 G, 100 mW m^{-2}. Their corresponding photovoltaic data are listed in Table 2. An increased PCE of 3.94 % with a J_{sc} of 8.80 mA cm^{-2} and a *FF* of 46.4% is observed in the TPA(BT-3Cz)$_3$-based solar cells under annealing at 110 ^{o}C, while the TPA(BT-2Cz)$_3$-based cells exhibited the maximum PCE of 3.11 % with a J_{sc} of 7.69 mA cm^{-2} and a *FF* of 40.4%. It is obvious that TPA(BT-3Cz)$_3$ exhibited better photovoltaic performance except the slightly low V_{oc} value in contrast to TPA(BT-2Cz)$_3$ in the OSCs. Therefore, our results here indicated that tuning the substituted position of carbazolyl at the molecular terminal could improve the photovoltaic performance for its SMs. Furthermore, appending the planar carbazolyl terminal group is also an efficient method to achieve the high-performance photovoltaic molecules.

Fig. 5 shows the external quantum efficiency curves (*EQE*) of the devices at the optimized conditions. The spectral response across the wavelength range of 325-675 nm is clearly observed for both devices. However, while TPA(BT-2Cz)$_3$-based device is replaced with TPA(BT-3Cz)$_3$-based device, the *EQE* is significantly increased from

View Article Online
DOI: 10.1039/C5TA00166H

a maximum value of 60% to 75%. It indicates that the photoelectron conversion process is more efficient in the TPA(BT-3Cz)$_3$-based device than the TPA(BT-2Cz)$_3$-based device. Higher *EQE* value is available for TPA(BT-3Cz)$_3$ to present better photovoltaic performance in the OSCs.

In order to further study why TPA(BT-3Cz)$_3$-based solar cells exhibited better performance, the surface morphologies of the TPA(BT-2Cz)$_3$ and TPA(BT-3Cz)$_3$ blending films with $PC_{71}BM$ under the optimized conditions were recorded by atomic force microscopy (AFM) and are illustrated in Fig. 6. The root-mean-square (RMS) roughness of 0.4 and 0.6 nm are exhibited for the TPA(BT-2Cz)$_3$ and TPA(BT-3Cz)$_3$ blending films, respectively. It implies that both blending films show fairly homo-geneous surface. However, nanoscopic fibrousphase separation is obviously observed in the TPA(BT-3Cz)$_3$ based blending film. This ordered fibrous morphology should be one of the reasons for the significantly improved J_{sc} and *FF* because the inter-fibrillar regions contributes to high exciton dissociation and charge transport efficiency.[37]

3.5 Holes mobility

The holes mobility of the blend films was measured by the space charge limited current (SCLC) method in the hole-only devices with a structure of ITO/PEDOT: PSS/Active Layer/Au, which were approximated by the Mott-Gurney equation:[38]

$$J = \frac{9\,\varepsilon_0\,\varepsilon_r\,\mu_e\,V^2}{8\,d^3}$$

Here J is the current density, ε_r is the molecular dielectric constant, ε_0 is the free-space permittivity (8.85×10^{-12} F/m), d is the thickness of blend films (96 nm and 85 nm for TPA(BT-2Cz)$_3$ and TPA(BT-3Cz)$_3$, respectively), $V = V_{appl}-V_{bi}$, V_{appl} is the applied potential, and V_{bi} is the built-in potential which results from the difference of the work function between the anode and the cathode. Fig. 7 displays the $J^{1/2}$-V curves of the hole-only TPA(BT-2Cz)$_3$ and TPA(BT-3Cz)$_3$-based devices. The corresponding holes mobility are listed in Table 2. The holes mobilities up to 7.9×10^{-5} and 9.0×10^{-5} $cm^2V^{-1}s^{-1}$ are exhibited in the hole-only TPA(BT-2Cz)$_3$ and TPA(BT-3Cz)$_3$-based devices, respectively. The observed higher hole mobility forTPA(BT-3Cz)$_3$ is also

View Article Online
DOI: 10.1039/C5TA00166H

available for the *FF* improvement in the TPA(BT- 3Cz)$_3$-based cells.

4. Conclusion

In conclusion, two TPA-cored star-shaped molecules of TPA(BT-2Cz)$_3$ and TPA-(BT-3Cz)$_3$ were obtained with 2- and 3-carbazolyl groups at terminals, respectively. Both SMs exhibited good thermal stability, broad spectral response region covering from 325 to 570 nm. Significantly increased photovoltaic performance was observed in the solution-processable organic solar cells based on TPA(BT-3Cz)$_3$ instead of TPA(BT-2Cz)$_3$. The maximum PCE of 3.94% with J_{sc} of 8.80 mA cm^{-2}, *FF* of 46.42% and V_{oc} of 0.97 V was obtained in the TPA(BT-3Cz)$_3$-based cell. Our results indicated that the structures and substituted positions of planar carbazolyl at terminals play a significant role in improving photovoltaic performance for its SMs in OSCs.

Acknowledgements

Thanks to the Financial Supports from the Major Program for Cultivation of the National Natural Science Foundation of China (91233112), the National Natural Science Foundation of China (21172187, 51403178, 51273168, 21202139), the Innovation Group and Xiangtan Joint Project of Hunan Natural Science Foundation (12JJ7002 and 12JJ8001), the Open Project for National Key Laboratory of Luminescent Materials and Devices (2014-skllmd-10), Research Foundation of Education Bureau of Hunan Province (13A102,14C1099) and the Hunan Postgraduate Science Foundation for Innovation (CX2014B257, CX2013B268).

Appendix A. Supplementary data

Supplementary data associated with this article can be found in the online version at http://dx.doi.org/xxx/xxx.

References

1 Y. F. Li, *Acc. Chem. Res.*, 2012, **45**, 723−733.

2 H. X. Zhou, L. Q. Yang and W. You, *Macromolecules*, 2012, **45**, 607−632.

3 J. E. Coughlin, Z. B. Henson, G. C. Welch and G. C. Bazan, *Acc. Chem. Res.*, 2014, **47**, 257−270.

View Article Online
DOI: 10.1039/C5TA00166H

4 Y. S. Chen, X. J. Wan and G. K. Long, *Acc. Chem. Res.*, 2013, **46**, 2645−2655.

5 G. Yu, J. Gao, J. C. Hummelen, F. Wudl and A. J. Heeger, *Science*, 1995, **270**, 1789−1791.

6 J. Y. Zhou, X. J. Wan, Y. S. Liu, Y. Zuo, Z. Li, G. R. He, G. K. Long, W. Ni, C. X. Li, X. C. Su and Y. S. Chen, *J. Am. Chem. Soc.*, 2012, **134**, 16345−16351.

7 J. Y. Zhou, Y. Zuo, X. J. Wan, G. K. Long, Q. Zhang, W. Ni, Y. S. Liu, Z. Li, G. R. He, C. X. Li, B. Kan, M. M. Li and Y. S. Chen, *J. Am. Chem. Soc.*, 2013, **135**, 8484−8487.

8 B. Kan, Q. Zhang, M. M. Li, X. J. Wan, W. Ni, G. K. Long, Y. C. Wang, X. Yang, H. R. Feng and Y. S. Chen, *J. Am. Chem. Soc.*, **136**,15529−15532.

9 X. F. Liu, Y. M. Sun, L. A. Perez, W. Wen, M. F. Toney, A. J. Heeger and G. C. Bazan, *J. Am. Chem. Soc.*, 2012, **134**, 20609−20612.

10 J. A. Love, I. Nagao, Y. Huang, M. Kuik, V. Gupta, C. J. Takacs, J. E. Coughlin, L.Qi, T. S. van der Poll, E. J. Kramer, A. J. Heeger, T. Q. Nguyen and G. C. Bazan, *J. Am. Chem. Soc*., 2014, **136**, 3597−3606.

11 Y. S. Liu, Y. Yang, C. C. Chen, Q. Chen, L. T. Dou, Z. R. Hong, G. Li and Y. Yang, *Adv. Mater.*, 2013, **25**, 4657–4662.

12 A. Ajayaghosh, *Chem. Soc. Rev*., 2003, **32**, 181–191.

13 C. H. Duan, F. Huang and Y. Cao, *J. Mater. Chem.*, 2012, **22**, 10416–10434.

14 S. Y. Ma, Y. Y. Fu, D. B. Ni, J. Mao, Z. Y. Xie and G. L. Tu, *Chem. Commun*., 2012, **48**, 11847–11849.

15 J. Zhang, Y. Yang, C. He, D. Deng, Z. B. Li and Y. F. Li, *J. Phys. D: Appl. Phys*., 2011, **44**, 475101–475105.

16. Z. Lu, C. H. Li, T. Fang, G. W. Li and Z. S. Bo, *J. Mater. Chem. A,* 2013, **1**, 7657–7665.

17. J. Zhang, D. Deng, C. He, Y. J. He, M. J. Zhang, Z. G. Zhang, Z. J. Zhang and Y. F. Li, *Chem*. *Mater*., 2011, **23**, 817–822.

18. Y. M. Zhang, X. C. Bao, M. J. Xiao, H. Tan, Q. Tao, Y. F. Wang, Y. Liu, R. Q. Yang and W. G. Zhu, *J. Mater. Chem. A*, 2015, **3**, 886–893.

19 Y. Z. Lin, P. Cheng, Y. F. Li and X. W. Zhan, *Chem. Commun.*, 2012, **48**,

View Article Online
DOI: 10.1039/C5TA00166H

4773–4775.

20 J. Y. Pan, L. J. Zuo, X. L. Hu, W. F. Fu, M. R. Chen, L. Fu, X. Gu, H. Q. Shi, M. M. Shi, H. Y. Li and H. Z. Chen, *ACS Appl. Mater. Interfaces*, 2013, **5**, 972−980.

21 W. Li, Q. D. Li, C. H. Duan, S. J. Liu, L.Ying, F. Huang and Y. Cao, *Dyes Pigm.*, 2015, **113**, 1–7.

22 H. X. Shang, H. J. Fan, Y. Liu, W. P. Hu, Y. F. Li and X. W. Zhan, *Adv. Mater.*, 2011, **23**, 1554–1557.

23 J. Zhang, J. T. Yu, C. He, D. Deng, Z. G. Zhang, M. J. Zhang, Z. B. Li and Y. F. Li, *Org. Electron.*, 2013, **13**, 166–172.

24 J. Zhang, Y. Yang, C. He, Y. J. He, G. J. Zhao and Y. F. Li, *Macromolecules*, 2009, **42**, 7619–7622.

25 Y. Y. Jiang, D. Yu, L. H. Lu, C. Zhan, D. Wu, W. You, Z. Z. Xie and S. Q. Xiao, *J. Mater. Chem. A,* 2013, **1**, 8270–8279.

26 W. Ni, M. M. Li, B. Kan, Y. Zuo, Q. Zhang, G. K. Long, H. R. Feng, X. J. Wan and Y. S. Chen, *Org. Electron.*, 2014, **15**, 2285–2294.

27 E. G. Wang, L. T. Hou, Z. Q. Wang, Z. F. Ma, S. Hellstrom, W. L. Zhuang, F. L. Zhang, O. Inganas and M. R. Andersson, *Macromolecules*, 2011, **44**, 2067–2073.

28 Y. H. Fu, H. Cha, G. Y. Lee, B. J. Moon, C. E. Park and T. Park, *Macromolecules*, 2012, **45**, 3004−3009.

29 H. C. Chu, D. Sahu, Y. C. Hsu, H. Padhy, D. Patra, J. Lin, D. Bhattacharya, K. L. Lu, K. H. Wei and H. C. Lin, *Dyes Pigm.*, 2012, **93**, 1488–1497.

30 K. Zhang, Y. T. Tao, C. L. Yang, H. You, Y. Zou, J. G. Qin and D. G. Ma, *Chem. Mater.*, 2008, **20**, 7324–7331.

31 J. Kim, Y. S. Kwon, W. S. Shin, S. J. Moon and T. Park, *Macromolecules*, 2011, **44**, 1909–1919.

32 D. F. Dang, P. Zhou, Q. Peng, K. Q. He, H. G. Jiang, P. G. Yang, H. Tan, Y. F. Wang, Y. Liu, G. T. Lei and W. G. Zhu, *Dyes Pigm.*, 2014, **109**, 6–12.

33 Y. H. Chen, Z. K. Du, W. C. Chen, Q. Liu, L. Sun, M. L. Sun and R. Q. Yang,*Org. Electron.*, 2014, **15**, 405–413.

34 D. F. Dang, M. J. Xiao, P. Zhou, J. W. Shi, Q. Tao, H. Tan, Y. F. Wang, X. C. Bao,

View Article Online
DOI: 10.1039/C5TA00166H

Y. Liu, E. G. Wang, R. Q. Yang and W. G. Zhu, *Org. Electron.*, 2014, **15**, 2876–2884.

35 C. M. Cardona, W. Li, A. E. Kaifer, D. Stockdale and G. C. Bazan, *Adv. Mater.,*2011, **23**, 2367–2371.

36 D. F. Dang, P. Zhou, J. Zhong, J. Fan, Z. R. Wang, Y. F. Wang, Y. Pei, X. C.Bao, R. Q. Yang, W. P. Hu and W. G. Zhu, *Polymer*, 2014, **55**, 6708–6716.

37 Y. Huang, X. Guo, F. Liu, L. J. Huo, Y. N. Chen, T. P. Russell, C. C. Han, Y. F. Li and J. H. Hou, *Adv. Mater.*, 2012, **24**, 3383–3389.

38 Y. Y Liang, D. Q. Feng, Y. Wu, S. T. Tsai, G. Li, C. Ray and L. P. Yu, *J. Am. Chem. Soc.*, 2009, **131**, 7792–7799.

View Article Online
DOI: 10.1039/C5TA00166H

Captions of Figures

Scheme 1. Synthetic routes of TPA(BT-2Cz)$_3$ and TPA(BT-3Cz)$_3$.

Fig. 1. The optimized geometries and electron-state-density distributions ofTPA(BT-2Cz)$_3$ and TPA(BT-3Cz)$_3$ using DFT method at the B3LYP/6-31G** level.

Fig. 2. Normalized UV–Vis absorption spectra of TPA(BT-2Cz)$_3$ and TPA(BT-3Cz)$_3$ in $CHCl_3$ solution and film state.

Fig. 3. Cyclic voltammograms of TPA(BT-2Cz)$_3$ and TPA(BT-3Cz)$_3$ film on Pt electrode.

Fig. 4. Current density-voltage characteristics of the TPA(BT-2Cz)$_3$ and TPA(BT-3Cz)$_3$ based OSCs in the optimized conditions under the illumination of AM 1.5 G 100 mW/cm^2.

Fig. 5. External quantum efficiency (*EQE*) curves of the TPA(BT-2Cz)$_3$ and TPA-(BT-3Cz)$_3$ basedOSCs devices under the optimized conditions.

Fig. 6. AFM topographies of the blend films for TPA(BT-2Cz)$_3$ and TPA(BT-3Cz)$_3$ with $PC_{71}BM$ under the optimized condition.

Fig. 7. $J^{1/2}$-V curves ofTPA(BT-2Cz)$_3$ and TPA(BT-3Cz)$_3$-based devices for the measurement of the hole mobility under the optimized conditions.

Table 1. Physicochemical properties of TPA(BT-2Cz)$_3$ and TPA(BT-3Cz)$_3$.

Table 2. Photovoltaic performance of OSCs based on TPA(BT-2Cz)$_3$ and TPA(BT-3Cz)$_3$ under the illumination of AM 1.5 G 100 mW/cm^2 and the holes mobility of both molecules measured by SCLC.

View Article Online
DOI: 10.1039/C5TA00166H

Scheme 1:

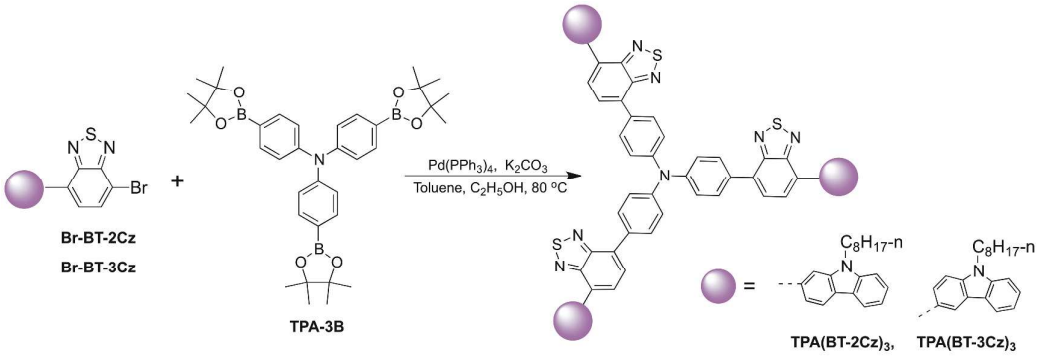

Fig. 1:

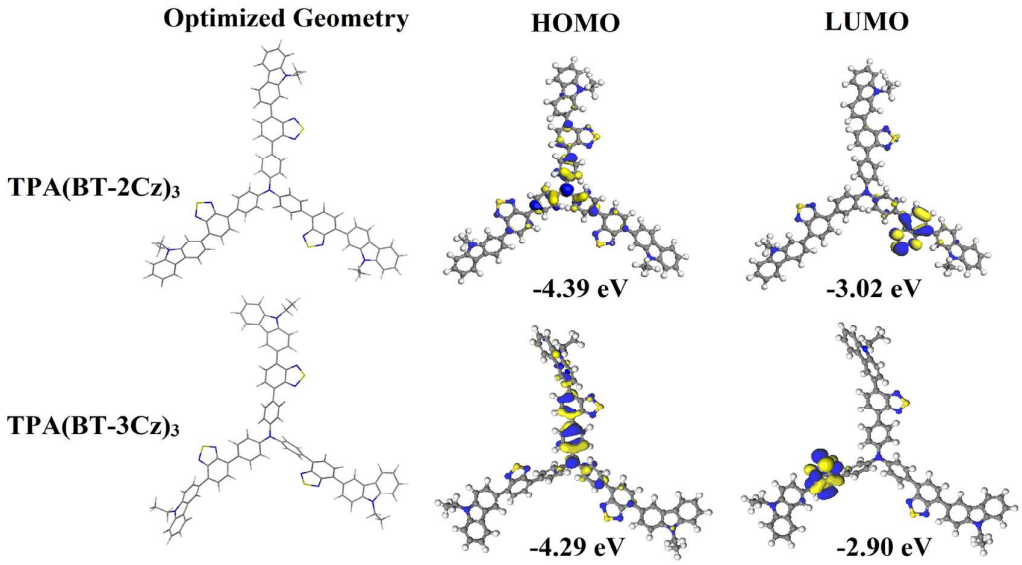

View Article Online
DOI: 10.1039/C5TA00166H

Fig. 2:

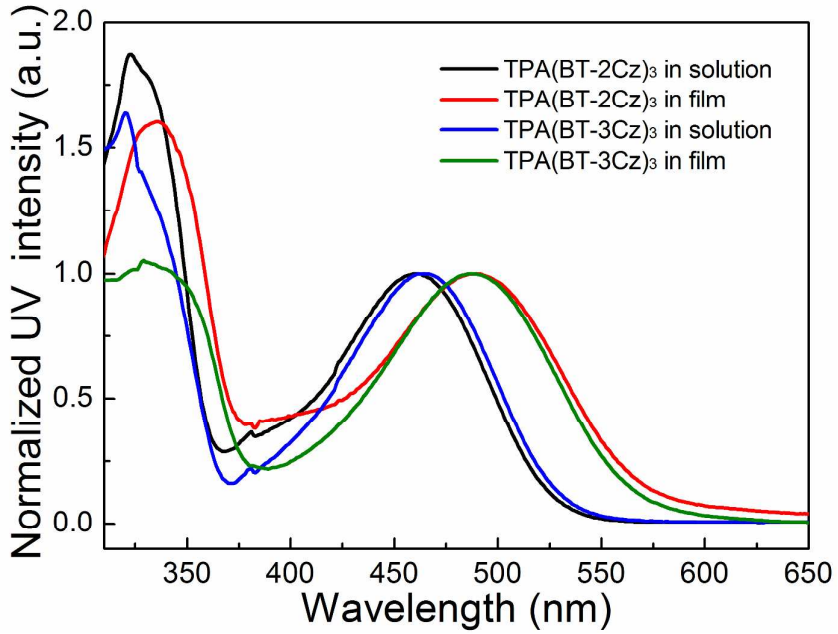

Fig. 3:

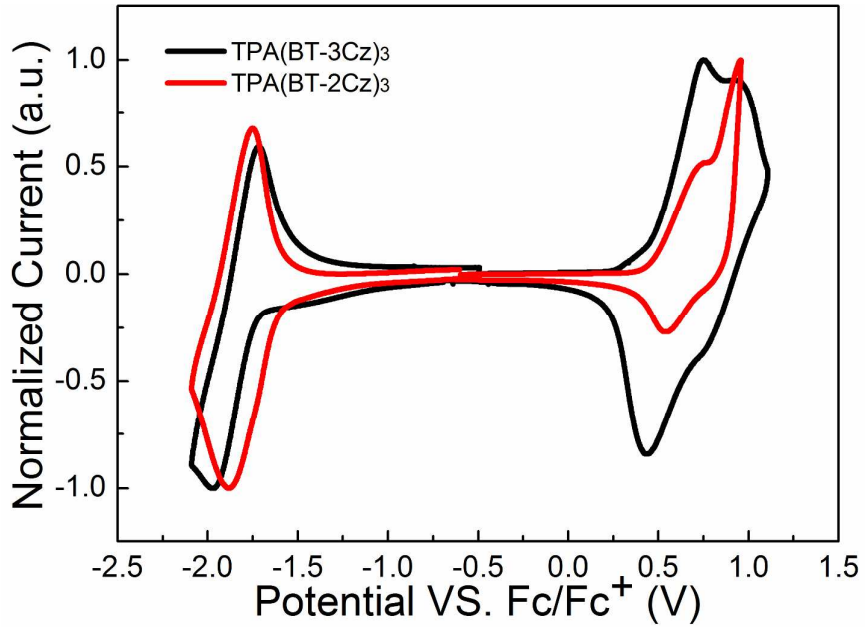

View Article Online
DOI: 10.1039/C5TA00166H

Fig. 4:

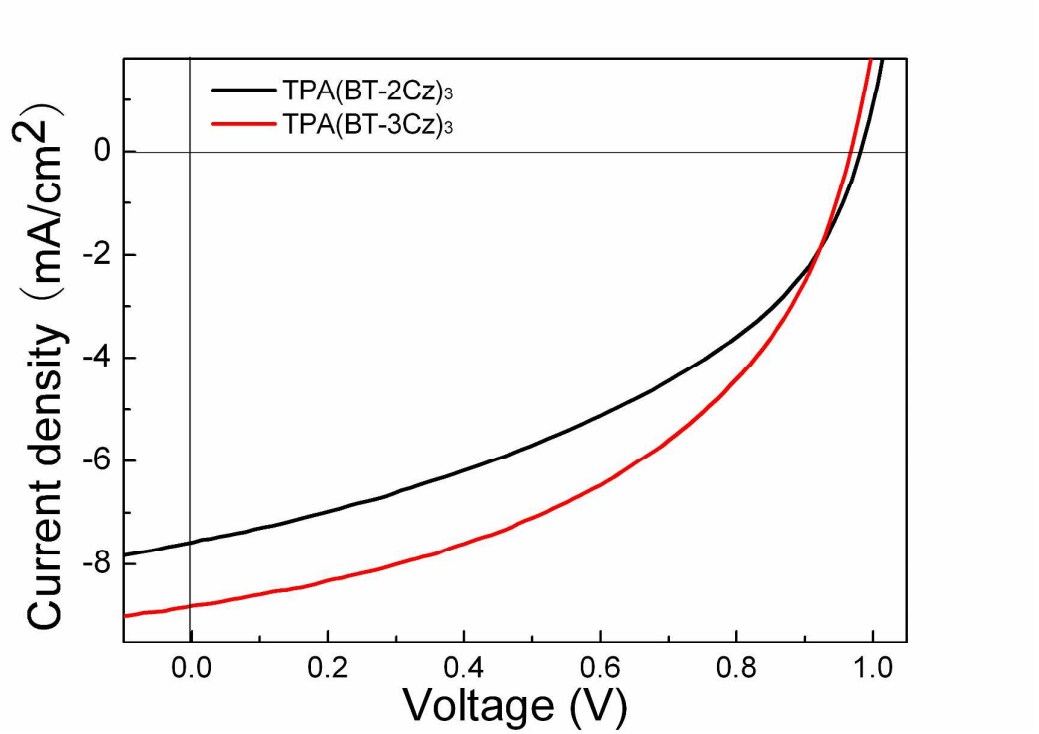

Fig. 5:

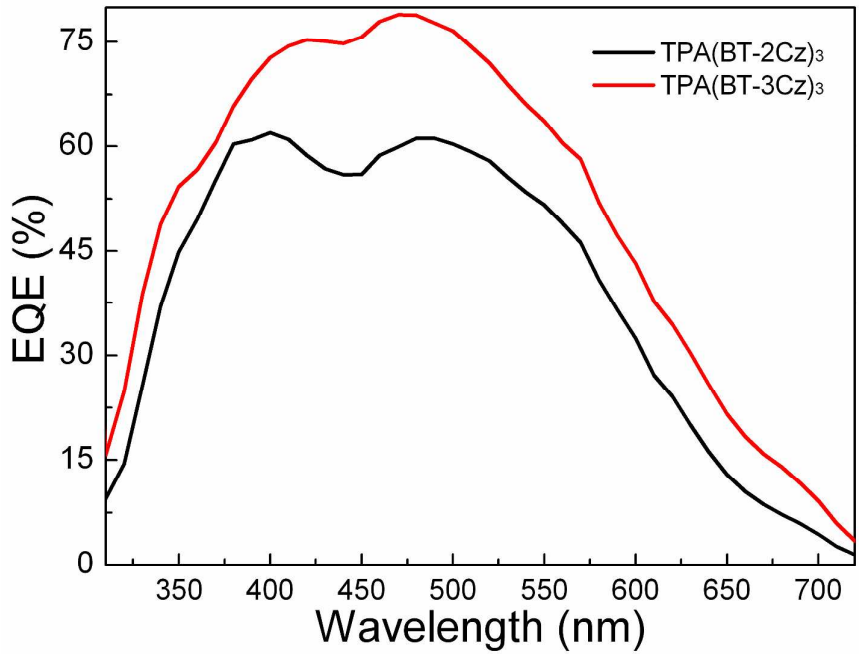

View Article Online
DOI: 10.1039/C5TA00166H

Fig. 6:

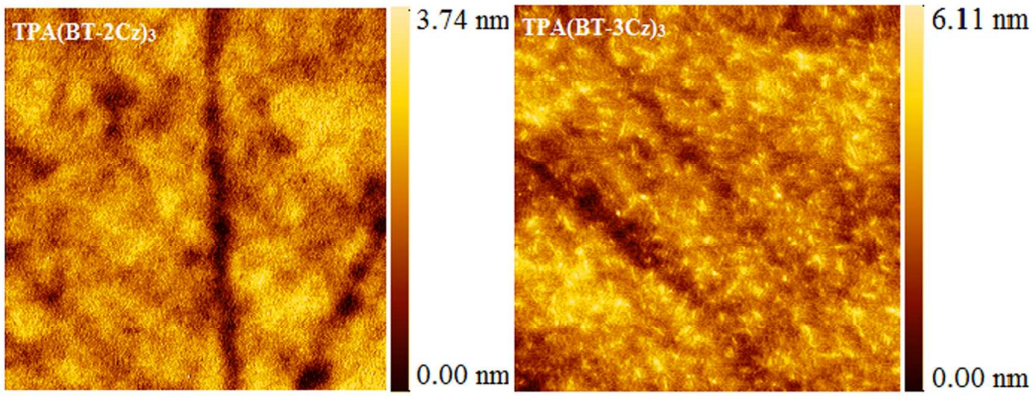

Fig. 7:

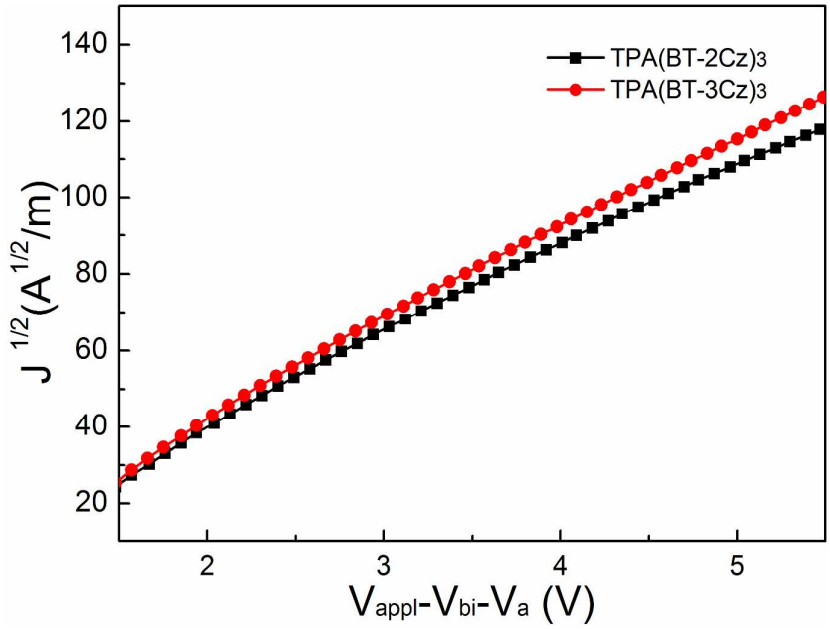

View Article Online
DOI: 10.1039/C5TA00166H

Table 1:

Compounds	λ_{abs} [a] (nm)	λ_{abs} [b] (nm)	E_g^{opt} (eV)	E_{HOMO} (eV)	E_{LUMO} (eV)	E_g^{cv}(eV)	T_d (^oC)
TPA(BT-2Cz)$_3$	322,460	334,490	2.15	-5.25	-3.24	2.01	469
TPA(BT-3Cz)$_3$	320,465	333,489	2.20	-5.18	-3.15	2.03	463

[a] measured in $CHCl_3$ solution; [b] measured in the neat film.

Table 2:

Active layer [a]	Blend ratios [b]	V_{oc} (V)	J_{sc} (mA/cm^2)	FF (%)	PCE (%)	Holes mobility (cm^{2}v^{-1}m^{-1})
TPA(BT-2Cz)$_3$	1:4	1.01	7.69	40.40	3.11	7.9×10^{-5}
TPA(BT-3Cz)$_3$	1:4	0.97	8.80	46.42	3.94	9.0×10^{-5}

[a] Blending with $PC_{71}BM$; [b]Annealed at 110 ^oC;

View Article Online
DOI: 10.1039/C5TA00166H

Table of Contents

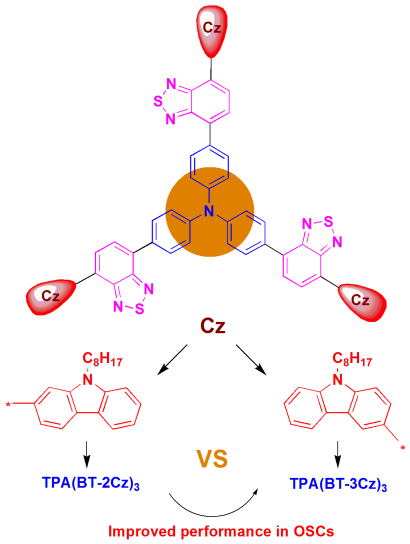

Significantly enhanced photovoltaic performance with PCE up to 3.94% was achieved by tuning the substituted positions of carbazolyl at terminal.